Computational Study on the Effect of Anode Layer Variation on the Performance of FASnI₃-based Perovskite Solar Cells

Febri Ariyanto^{1, 2}, Rossyaila Matsna Muslimawati³, Mohammad Kemal Augusta⁴, Muhammad Haris Mahyuddin^{4,*}

Abstract. The development of lead-free perovskite solar cells (PSC) is gaining traction due to concerns over the toxicity of lead-based materials. This study explores various anode materials as back contact of tin-based perovskites with a complete configuration consisting of FTO/TiO₂/FASnI₃/PTAA/Anode to optimize the performance of FASnI₃-based PSC. Using SCAPS-1D and density functional theory (DFT) simulations, we analyze the impact of varying work functions of various metals, including several alloy metals, on the device's performance and stability. The simulation results indicate that variations in the work function of metal contacts ranging from 4.3 eV to 5.0 eV affect the Power Conversion Efficiency (PCE) of the PSC. Utilizing DFT calculations enables the confirmation of the accuracy of the work function parameter by computing the difference between vacuum potential and Fermi energy, further validating the device's capability with PCE up to 17%. These results highlight the significance of selecting suitable anode materials to improve both the efficiency and durability of

Keywords: *DFT*, *FASnI*₃, lead-free perovskite, metal back contact, photovoltaic stability, power conversion efficiency, SCAPS-1D.

tin-based PSCs based on their layer configuration. Key properties of the anode material, such as work function and electrical conductivity, can optimize the

1 Introduction

The development of lead-free PSC has garnered significant attention due to environmental and sustainability concerns surrounding lead-based materials [1]. Among lead-free alternatives, tin-based perovskites, such as formamidinium tin triiodide (FASnI₃), have emerged as promising candidates for absorber layers due

Received ______, Revised _____, Accepted for publication _____ Copyright © xxxx Published by ITB Journal Publisher, ISSN: xxxx-xxxx, DOI: 10.5614/xxxx

charge extraction, enhancing overall device performance.

¹ Master Program of Engineering Physics, Faculty of Industrial Technology, Institut Teknologi Bandung, Jl. Ganesha No. 10 Bandung 40132, Indonesia.

² Various Renewable Energy Division of PT. PLN (Persero) Head Office, Jl. Trunojoyo Blok M-I No.135, Jakarta Selatan 12160, Indonesia.

³ Doctoral Program of Engineering Physics, Faculty of Industrial Technology, Institut Teknologi Bandung, Jl. Ganesha No. 10 Bandung 40132, Indonesia.

⁴ Quantum and Nano Technology Research Group, Faculty of Industrial Technology, Institut Teknologi Bandung, Jl. Ganesha No. 10 Bandung 40132, Indonesia.
*Email: mahyuddin133@itb.ac.id

to their suitable optoelectronic properties [2]. Perovskite solar cells operate in three main steps: photogeneration of charge carriers, charge transport, and charge extraction. Tin-based perovskites, with a low bandgap range of 1.1 to 1.3 eV, are capable of absorbing both visible and infrared light, leading to the generation of charge carriers (electrons and holes) [3]. This generates charge carriers (electrons and holes) which are separated by energy band alignment between the perovskite and the electron or hole transport layers. It's crucial to find the suitable band alignment between each layer. The use of noble metals like gold and platinum as back contact electrodes is still considerably expensive and challenging to develop as a commercially viable option [4]. Several experimental and computational studies have been done to obtain the supporting anode materials properties and possible to have viable production cost using alternative materials like a low melting point metal alloy (Wood's alloy) as top electrodes achieving 14.8% PCE in Pb-based PSC [5] or introducing metal salt (Al, Ca, and Mg) on a carbon-based counter electrode to improve the energy level alignment, hole extraction efficiency, and reducing charge recombination [6].

Among metal-based materials, there are few that are commonly used as back contact electrodes in solar cell applications. Metals suitable for solar cell back contact should have good electrical conductivity and chemical stability [7]. Nickel is shown to be corrosion-resistant and thus capable of preventing oxidation and degradation over time [8, 9]. Cobalt, though conductive, exhibits moderate chemical stability and is more prone to oxidation, particularly in humid conditions [10]. Copper, while offering good conductivity, is found to be susceptible to rapid oxidation and diffusion into perovskite layers, negatively impacting the perovskite's structural and electronic properties [9, 10]. Meanwhile, the alloy metals AgAl, with silver's high conductivity and aluminum's resistance to oxidation, hypothetically provides good stability and compatibility with perovskite materials [11]. SnBi, although conductive and lowcost, has relatively lower chemical stability due to tin's susceptibility to oxidation, potentially leading to faster degradation [12]. CoCrNi also indicates good conductivity; however, the development of CoCrNi as an alloy material in solar cell applications is still strictly limited, and there is no indication of mass manufacturing availability.

In this study, we employ FASnI₃ as the absorber layer, FTO as the front contact electrode, TiO₂ as the electron transport layer (ETL) [13, 14], and PTAA as the hole transport layer (HTL) [15] to investigate the suitable anode materials to improve both the efficiency of tin-based PSCs and figuring the key properties of the anode material for optimizing charge extraction and minimizing recombination losses. SCAPS-1D simulation and density functional theory (DFT) are utilized to examine PSC performance and the anode electrical properties using anode materials, including Cu, Co, Ni, AgAl, SnBi, and CoCrNi

as they typically possess the characteristics of good electrical conductivity reflected in their work function value which aligned with hole transporting layer, achieving conversion performance (PCE) within range 3 to 17%.

2 Methodology

The SCAPS-1D simulation was conducted using a layered model of the Perovskite Solar Cell (PSC), as depicted in Figure 1. This model is based on an experimentally developed FASnI₃-based photovoltaic (PV) device with a similar configuration using Gold (Au) as back contact [16]. The basic parameters were validated through a reverse simulation method from the J-V curve. The basic parameters were optimized based on published works to improve the simulated performance [13, 15, 17].

A heterojunction architecture FTO/TiO₂/FASnI₃/PTAA/Anode was explored to enhance device performance. The physical parameters for the ETL, HTL, absorber, and FTO layers are outlined in Table 1. Uniform values were assumed for certain parameters, such as the thermal velocities and interface defects. Table 2 provides the defect densities within the absorber and at the interfaces. The front contacts work function was adjusted to ensure flat band conditions, while the back metal work function varies based on material.

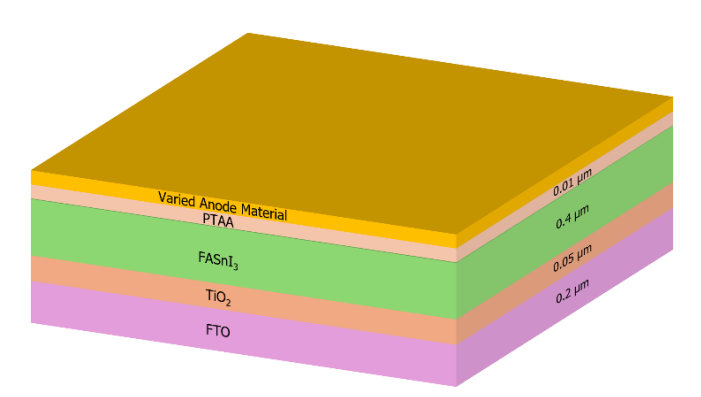


Figure 1 Configuration of FASnI3-based PSC

The density functional theory (DFT) computational simulations were modeled for each anode materials in Table 3. The computation began with structure optimization to determine the stable configuration.

Parameters	FTO [17]	TiO ₂ [13,14]	FASnI ₃ [13, 14]	PTAA [15]
Thickness (nm)	200	50	400	10
Bandgap (eV)	3.6	3.2	1.377	3.2
Electron affinity (eV)	4.1	4.1	4.2	2.13
Dielectric permittivity	10	55	8.2	3
CB effective density of states (cm ⁻³)	2.2×10^{18}	1×10^{21}	2.2×10^{18}	2×10^{18}
VB effective density of states (cm ⁻³)	1.8×10^{19}	2×10^{20}	1.8×10^{19}	2×10^{18}
Electron mobility cm ² / Vs	100	0.006	1.6	0.001
Hole mobility cm ² / Vs	25	0.006	1.6	0.001
Shallow donor density, ND (cm ⁻³)	1×10^{20}	1×10^{21}	0	0
Shallow acceptor density, NA (cm ⁻³)	0	0	1×10^{21}	1×10^{21}
Electron thermal velocity (cm/s)	1.00×10^{15}	1.00×10^{15}	1.00×10^{13}	1.00×10^{15}
Hole thermal velocity (cm/s)	1.00×10^{7}	1.00×10^{7}	1.00×10^{7}	1.00×10^{7}

Table 1 Physical parameters used in SCAPS-1D simulation

Table 2 Defect parameter used in SCAPS-1D simulation

Parameters	FTO [17]	TiO ₂ [13, 14]	FASnI ₃ [13, 14]	PTAA [15]	TiO ₂ / FASnI ₃	FASnI ₃ / PTAA
Defect type	Neutral	Single Acceptor	Single Donor	Single Donor	Neutral	Neutral
Energetic distribution	Single	Single	Single	Single	Single	Single
Reference for defect energy level Et	Above EV (SCAPS < 2.7)	Above EV (SCAPS < 2.7)	Above EV (SCAPS < 2.7)	Above EV (SCAPS < 2.7)	Above the highest EV	Above the highest EV
Nt Total (1/cm ³)	1.0×10^{15}	1.0×10^{15}	1.0×10^{13}	1.0×10^{15}	1.0×10^{12}	1.0×10^{12}

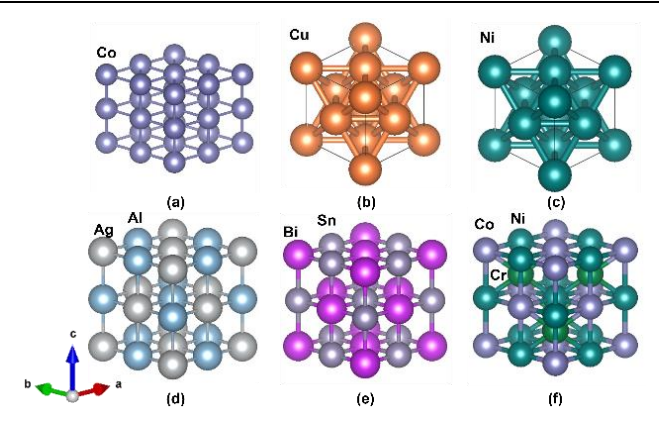


Figure 2 Crystal structure of anode materials (a) Co, (b) Cu, (c) Ni, (d) AgAl, (e) SnBi, and (f) CoCrNi.

Spin-polarized density functional theory (DFT) calculations were performed for all anode materials shown in Figure 2 within the Kohn–Sham framework [18, 19] using the Vienna Ab-initio Simulation Package (VASP) [20, 21]. The interaction

between ion cores and electrons was modeled through the Projector Augmented Wave (PAW) method [22, 23]. For exchange-correlation, the Perdew-Burke-Ernzerhof (PBE) functional [24] under the generalized gradient approximation (GGA) was employed, offering a reliable balance between accuracy and computational efficiency. The rotationally invariant GGA+U approach by Dudarev et al. [25] was applied, with an effective Hubbard parameter $U_{\rm eff}$ of 4.0 to 6.0 eV for the transition metal, as recommended by Rosen et al [26]. Plane wave basis sets were set with a 500 eV cutoff energy for all calculations [27]. Brillouin zone sampling, centred at the Γ point, was configured to a 2×2×2 grid using the Monkhorst-Pack scheme. The D3 method with zero damping accounted for dispersion corrections [28]. Cell optimizations employed the conjugate gradient method, converging when atomic forces were below 0.01 eV/Å, allowing full relaxation of all atoms during calculations.

The work-function, ϕ , was defined as the minimum amount of external energy required to move an electron with the Fermi energy from the surface of an electrode or crystal to the field-free region external to the surface at absolute zero [29]. It characterizes the ability of a metal-based back contact to facilitate hole extraction. It is defined theoretically as the energy difference between the vacuum potential (ϕ_{vacuum}), the Fermi level (ϵ_{Fermi}) of the metal surface, and ϵ is the electron charge:

$$\Phi = e\phi_{vacuum} - \varepsilon_{Fermi}$$

The computational work function value was investigated by ensuring that the structure had a sufficiently large atom-free region-charge-density-free and field-free in the direction normal to the surface. A general guideline was to center the atoms in the cell and maintain between 8–12 Å of vacuum on either side in this direction [30]. The modeled structure is shown in Figure 3 below.

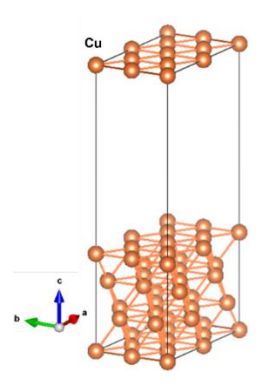


Figure 3 Slab model of metal-based back contact materials with additional vacuum space 8-12 Å to c-axis direction.

3 Result and Discussion

3.1 Electronic Properties of Anode Materials

The reference value of metal's work function as electronic properties of metal materials can be determined through various experimental measurement methods. Table 3 shows the average work function of the metals used in this study from multiple available research sources.

Table 3 Reference value of work function for metal-based anode materials

Material	Work Function (eV)	Reference	
Co	5.00		
Cu	4.70		
Ni	5.01	[11, 12, 29, 31 - 38]	
AgAl	4.70		
SnBi	5.11		
CoCrNi	5.10		

Based on the DFT output results presented in the Table 4, the surface energy characteristics of various metal materials can be analyzed, focusing on their work function (WF), Fermi energy (Energy Fermi), and vacuum level.

Table 4 Summary of DFT computational result for varied metal-based back contacts materials.

Material	Energy Fermi	Vacuum Level	Work Function (eV)
Cu	0.97	5.83	4.86
Co	1.92	6.83	4.91
Ni	1.39	6.43	5.03
AgAl	2.44	7.06	4.61
SnBi	0.42	4.78	4.36
CoCrNi	-0.002	4.925	4.923

CoCrNi has a negative value of Fermi energy. However, this doesn't imply that the material has less than zero energy but rather that the highest occupation levels are identified at the negative axis. The energy Fermi is only relevant to the characteristic of electron flow through the materials; the determination of an anode's energy alignment is based on work function parameters that directly impact the characteristics of the metal to inject or extract charges at the interface with other materials. Anode is directly contacted with HTL, which has an electron affinity of 2.13 eV as the maximum position of the conduction band (CBM), with a band gap of 3.2 eV, implying the gap between CBM and VBM are 2.13 to -1.07 eV. Ideally, the work function of the anode should align closely to VBM of HTL

material, which consists of Co, Cu, Ni, and CoCrNi based on DFT calculations on Table 4.

3.2 Effect of Metal Work Function

The SCAPS-1D simulation uses the AM 1.5G solar spectrum with an incident power density of 100 mW/cm² at 300 K to illuminate the proposed PV structure, varying Co, Cu, Ni, AgAl, SnBi, and CoCrNi as back contact electrodes with different work functions. The energy band diagram (a) is projected based on the parameters in Table 1, showing the position of the valence band relative to the conduction band for each layer. Energy band diagram (b) was derived from SCAPS-1D model using DFT-result of anode's work function.

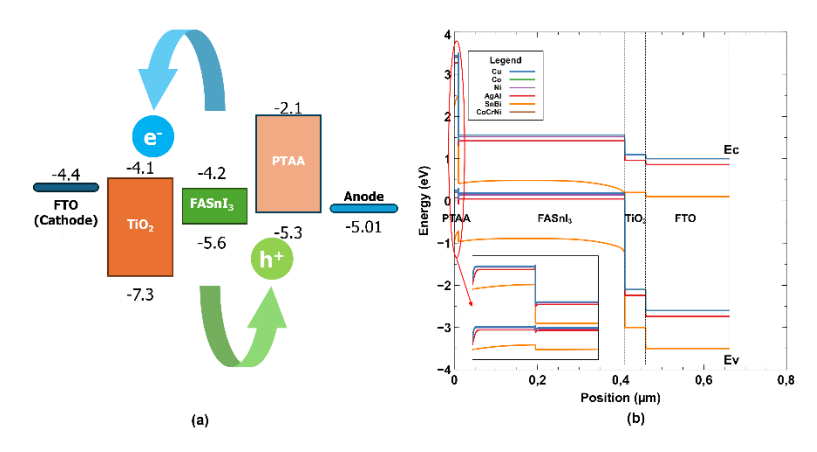


Figure 4 (a) Energy band diagram for FTO/TiO₂/FASnI₃/PTAA/Anode based on reference parameters (b) Modelled energy diagram with six (6) different back contact using SCAPS.

By inputting these DFT-derived work functions into SCAPS-1D, it can refine the energy band alignment between the hole transport layer (HTL), as seen in Figure 4 (a) Energy band diagram for FTO/TiO₂/FASnI₃/PTAA/Anode based on reference parameters (b) Modelled energy diagram with six (6) different back contact using SCAPS. (b), allowing for a more precise prediction of overall device performance. The efficiency of hole collection in an n-i-p structured perovskite solar cell (PSC), such as FTO/TiO₂/FASnI₃/PTAA/Anode, depends on the properties of the back contact material. The simulation results show that increasing the work function improves the current density-voltage (J-V) characteristics.

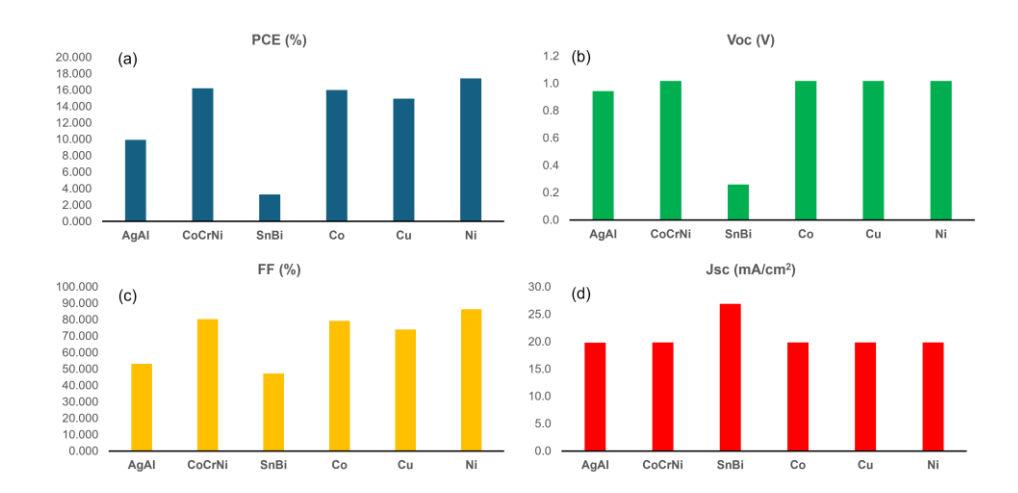


Figure 5 (a) PCE, (b) V_{oc}, (c) FF, and (d) J_{sc} of FASnI₃-based devices with varying back contact material.

The result comparison shows that back contact materials with higher work functions, such as Ni and CoCrNi, deliver the best performance, demonstrated by higher PCE, $V_{\rm oc}$, and FF values. Higher work function materials promote favorable band bending, effectively blocking electrons and enhancing hole collection, thus boosting $V_{\rm oc}$ and FF. Nickel (Ni) displays the highest computed work function of 5.03 eV, which has the closest distance with or slightly exceeding the valence band maximum of the HTL and minimizing the barrier for hole extraction.

Configuration	J _{sc} (mA/cm ²)	V _{oc} (V)	FF (%)	PCE (%)
FTO/TiO ₂ /FASnI ₃ /PTAA/Cu	19.835	1.0170	74.09	14.95
FTO/TiO ₂ /FASnI ₃ /PTAA/Co	19.836	1.0174	79.13	15.97
FTO/TiO ₂ /FASnI ₃ /PTAA/Ni	19.838	1.0176	86.35	17.43
FTO/TiO ₂ /FASnI ₃ /PTAA/AgAl	19.822	0.943	53.20	9.94
FTO/TiO ₂ /FASnI ₃ /PTAA/SnBi	26.923	0.259	47.18	3.29
FTO/TiO ₂ /FASnI ₃ /PTAA/CoCrNi	19.837	1.018	80.39	16.23

Table 5 Refined result of device performance simulations.

4 Conclusion

The investigation into various metal back contact materials with work functions ranging from 4.86 to 5.03 eV, including Cu, Co, Ni, AgAl, SnBi, and CoCrNi, are particularly effective in optimizing key performance parameters such as open-circuit voltage (V_{oc}) and fill factor (FF), leading to enhanced overall power

conversion efficiency (PCE) of 17.43% achieved at WF: 5.03 eV with Ni materials, due to their suitable energy band alignment.

5 Reference

- [1] "Best Research-Cell Efficiency Chart | Photovoltaic Research | NREL." 6 October 2024. [Online]. https://www.nrel.gov/pv/cell-efficiency.html.
- [2] J. O. Obila, H. Lei, E. O. Ayieta, A. A. Ogacho, B. O. Aduda, & F. Wang, *Optoelectronic property refinement of FASnI₃ films for photovoltaic application*, Materials Letters, 300, 1 October 2021, doi: 10.1016/j.matlet.2021.130099.
- [3] M. Dawson, C. Ribeiro, & M. R. Morelli, *A Review of Three-Dimensional Tin Halide Perovskites as Solar Cell Materials*, Universidade Federal de Sao Carlos, 12 January 2022, doi: 10.1590/1980-5373-MR-2021-0441.
- [4] R. Vidal, J. A. Alberola-Borràs, N. Sánchez-Pantoja, and I. Mora-Seró, Comparison of Perovskite Solar Cells with other Photovoltaics Technologies from the Point of View of Life Cycle Assessment, John Wiley and Sons Inc. 1 May 2021, doi: 10.1002/aesr.202000088.
- [5] Elizaveta E. Vaneeva, Victoria V. Ozerova, Sergey A. Tsarev, Mohamed M. Elnaggar, Nadezhda N. Dremova, Sergey L. Nikitenko, & Pavel A. Troshin, *Low melting point metal alloys for cost-efficient deposition of electrodes in perovskite solar cells*, Synthetic Metals, 293, 1 March 2023, doi: 10.1016/j.synthmet.2023.117301.
- [6] M. F. Don, P. Ekanayake, J. R. Jennings, H. Nakajima, U. Kumar D, and C. M. Lim, *Influence of metal salts (Al, Ca, and Mg) on the work function and hole extraction at carbon counter electrodes in perovskite solar cells*, Heliyon, 9 (7), 1 July 2023, doi: 10.1016/j.heliyon.2023.e17748.
- [7] R. S. Hall, D. Lamb, and S. J. C. Irvine, *Back contacts materials used in thin film CdTe solar cells—A review*, John Wiley and Sons Ltd. 9(5), 01 May 2021, doi: 10.1002/ese3.843.
- [8] Marand, Z.R., Kermanpur, A., Karimzadeh, F., Barea, E.M., Hassanabadi, E., Anaraki, E.H., Julián-López, B., Masi, S., & Mora-Seró, I. Structural and Electrical Investigation of Cobalt-Doped NiO_x/Perovskite Interface for Efficient Inverted Solar Cells, Nanomaterials, 10(5), 1 May 2020, doi: 10.3390/NANO10050872.
- [9] J. H. Lee, Y. W. Noh, I. S. Jin, S. H. Park, & J. W. Jung, Efficient perovskite solar cells with negligible hysteresis achieved by sol-gel-driven spinel nickel cobalt oxide thin films as the hole transport layer, Journal of Materials Chemistry C, 7(24), pp. 7288–7298, 22 April 2019, doi: 10.1039/c9tc00902g.

- [10] N. M. Abdulmalek & H. A. Jawad, Influence of cobalt doping on structural and optical properties of copper oxide expected as an inorganic hole transport layer for perovskite solar cell, Journal of Materials Science: Materials in Electronics, 35(2), 1 January 2024, doi: 10.1007/s10854-024-11932-x.
- [11] Luo, Y., Chen, X., Zhang, C., Li, J., Shi, J., Sun, Z., Wang, Z., & Huang, S., *AgAl alloy electrode for efficient perovskite solar cells, RSC Advances*, 5(69), pp. 56037–56044, 23 June 2015, doi: 10.1039/C5RA06133D.
- [12] S. Han, F. Wu, W. Qin, H. Cao, L. Yang, and S. Yin, *Perovskite solar cell based on double-layer Ag/SnBi alloy as cathode*, Journal of Alloys and Compound, 888, 25 December 2021, doi: 10.1016/j.jallcom.2021.161455.
- [13] Almufarij, R. S., Ashfaq, A., Tahir, S., Alqurashi, R. S., Ragab, A. H., El-Refaey, D. E., Mushtaq, S., Shokralla, E. A., Ali, A., Capangpangan, R. Y., & Alguno, A. C., *Improving performance and recombination losses in lead free formamidinium tin based perovskite solar cells*, Materials Chemistry and Physics, 307, 1 October 2023, doi: 10.1016/j.matchemphys.2023.128150.
- [14] A. Hosen, M. S. Mian, & S. R. Al Ahmed, *Improving the Performance of Lead-Free FASnI*₃-Based Perovskite Solar Cell with Nb₂O₅ as an Electron Transport Layer, Advanced Theory and Simulations, 6(2), p. 2200652, 1 February 2023, doi: 10.1002/adts.202200652.
- [15] S. Ravishankar, Z. Liu, U. Rau, & T. Kirchartz, Electronic Supplementary Information Multilayer Capacitances: How Selective Contacts Affect Capacitance Measurements of Perovskite Solar Cells., submitted for publication. (Pending Publication), 17 October 2024. [Online]. http://dx.doi.org/10.48550/arXiv.2106.05758
- [16] Ke, W., Stoumpos, C. C., Zhu, M., Mao, L., Spanopoulos, I., Liu, J., Kontsevoi, O. Y., Chen, M., Sarma, D., Zhang, Y., Wasielewski, M. R., & Kanatzidis, M. G., *Enhanced photovoltaic performance and stability with a new type of hollow 3D perovskite {en}FASnI₃*, Science Advance, 3(8), p. e1701293, 30 August 2017, https://doi.org/10.1126/sciadv.1701293
- [17] S. Alireza Rasoli, S. Salmani, and S. Salmani, *Simulation and investigation of perovskite solar cell based on FASnI*₃ absorber layer, 29 January 2023. Innovation and Research in Engineering Sciences. https://www.researchgate.net/publication/367525324
- [18] P. Hohenberg & W. Kohn, *Inhomogeneous Electron Gas*, 136. Physical Review, 1964, pp. B864-B871, https://doi.org/10.1103/PhysRev.136.B864
- [19] W. Kohn & L. J. Sham, *Self-Consistent Equations Including Exchange and Correlation Effects*, 140. Physical Review, 1965, pp. A1133-1138, https://doi.org/10.1103/PhysRev.140.A1133
- [20] G. Kresse & J. Furthmüller, Efficiency of Ab-Initio Total Energy Calculations for Metals and Semiconductors Using a Plane-Wave Basis

- *Set*, 6 (1). Computational Material Science, 1996, pp. 15-50, https://doi.org/10.1016/0927-0256(96)00008-0
- [21] G. Kresse & J. Furthmüller, Efficient Iterative Schemes for Ab Initio Total-Energy Calculations Using a Plane-Wave Basis Set, 54. Physical Review B: Condensed Matter Material Physics, 1996, pp. 11169-11186, https://doi.org/10.1103/PhysRevB.54.11169
- [22] P. E. Blöchl, *Projector Augmented-Wave Method*, 50. Physical Review B: Condensed Matter Material Physics, 1994, pp. 17953-17979, https://doi.org/10.1103/PhysRevB.50.17953
- [23] G. Kresse & D. Joubert, From Ultrasoft Pseudopotentials to the Projector Augmented-Wave Method, 59. Physical Review B: Condensed Matter Material Physics, 1999, pp. 1759-1775, https://doi.org/10.1103/PhysRevB.59.1758
- [24] J. P. Perdew, K. Burke, & M. Ernzerhof, *Generalized Gradient Approximation Made Simple*, 77. Physical Review Letters, 1996, pp. 3865-3868, https://doi.org/10.1103/PhysRevLett.77.3865
- [25] S. L. Dudarev, S. Y. Savrasov, C. J. Humphreys, & A. P. Sutton, *Electron-Energy-Loss Spectra and the Structural Stability of Nickel Oxide: An LSDA+U Study*, 57. Physical Review B: Condensed Matter Material Physics, 1998, pp. 1505-1509, https://doi.org/10.1103/PhysRevB.57.1505
- [26] A. S. Rosen, J. M. Notestein, & R. Q. Snurr, Comparing GGA, GGA+U, and meta-GGA functionals for redox-dependent binding at open metal sites in metal-organic frameworks, Journal of Chemical Physics, 152, p. 40, 2020, doi: 10.1063/5.0010166.
- [27] H. J. Monkhorst & J. D. Pack, Special Points for Brillouin-Zone Integrations, 13. Physical Review B, 1976, pp. 5188-5192, https://doi.org/10.1103/PhysRevB.13.5188.
- [28] S. Grimme, J. Antony, S. Ehrlich, & H. A. Krieg, *Consistent and Accurate Ab Initio Parametrization of Density Functional Dispersion Correction* (*DFT-D*) for the 94 Elements H-Pu, 132. Journal of Chemical Physics, 2010, p. 154104, https://doi.org/10.1063/1.3382344
- [29] D. Etor, M. Ekele, & I. A. Akintunde, *Impact of Metal Work-Function on Current Rectification by Metal-Insulator-Metal Diodes*, FUOYE Journal of Engineering and Technology, 7(4), 28 December 2022, doi: 10.46792/fuoyejet.v7i4.886.
- [30] "Computing the work function VASP Wiki." 13 October 2024. [Online]. https://www.vasp.at/wiki/index.php/Computing_the_work_function
- [31] G. J. Evans, ECE Applied to Energy from Space-Time: Amplification of the Radiative Correction by Spin Connection Resonance, Journal of Foundations of Physics and Chemistry, 1(5), 2008.
- [32] S. Liu, H. Lu, & D. Y. Li, The relationship between the electron work function and friction behavior of passive alloys under different conditions,

- Applied Surface Science, 351, pp. 316–319, 1 October 2015, doi: 10.1016/J.APSUSC.2015.05.125.
- [33] I. Brodie, S. H. Chou, & H. Yuan, A general phenomenological model for work function, Surface Science, 625, pp. 112–118, 3 March 2014, doi: 10.1016/J.SUSC.2014.03.002.
- [34] H. Kawano, Effective work functions for ionic and electronic emissions from mono- and polycrystalline surfaces, Progress in Surface Science, 83(1–2), pp. 1–165, February 2008, doi: 10.1016/J.PROGSURF.2007.11.001.
- [35] Y. Luo, Y. Tang, L. Guo, & D. Y. Li, *Microstructure electron work function relationship: A crucial step towards 'electronic metallurgy*,' Materials Today Community, 26, p. 101977, March 2021, doi: 10.1016/J.MTCOMM.2020.101977.
- [36] H. Lu, X. Huang, R. Hou, & D. Y. Li, Understanding the Effect of Ni on Mechanical and Wear Properties of Low-Carbon Steel from a View-Point of Electron Work Function, Metallurgical and Material Transactions A-Physical Metallurgy Materials Science, 49(7), pp. 2612–2621, July 2018, doi: 10.1007/S11661-018-4616-1.
- [37] H. B. Michaelson, *The work function of the elements and its periodicity*, Journal of Applied Physics, 48(11), pp. 4729–4733, November 1977, doi: 10.1063/1.323539.
- [38] Jiang, Z., Chen, X., Lin, X., Jia, X., Wang, J., Pan, L., Huang, S., Zhu, F., & Sun, Z., *Amazing stable open-circuit voltage in perovskite solar cells using AgAl alloy electrode*, Solar Energy Materials and Solar Cells, 146, pp. 35–43, March 2016, doi: 10.1016/j.solmat.2015.11.026.

Acknowledgment

The authors are grateful to PT. PLN (Persero) for the financial and scholarship support provided throughout this research.